ACS APPLIED MATERIALS & INTERFACES

Research Article

www.acsami.org

Double-Wall TiO_2 Nanotube Arrays: Enhanced Photocatalytic Activity and *In Situ* TEM Observations at High Temperature

Chaorui Xue,[†] Takashi Narushima,[†,§] Yohei Ishida,[†] Tomoharu Tokunaga,[‡] and Tetsu Yonezawa*[,†]

[†]Division of Materials Science and Engineering, Faculty of Engineering, Hokkaido University, Kita 13, Nishi 8, Kita-ku, Hokkaido, Sapporo 060-8628, Japan

[‡]Department of Quantum Engineering, Graduate School of Engineering, Nagoya University, Furo-cho, Chikusa-ku, Aichi, Nagoya 464-8603, Japan

Supporting Information

ABSTRACT: By decreasing the water content in an NH_4F and glycerol−water electrolyte, the transition from single-wall to double-wall TiO_2 nanotube arrays was successfully achieved using an anodization method. The double-wall TiO_2 nanotube structures exhibited better photocatalytic activity than the typical single-wall structures. After modification with platinum nanoparticles, the photocatalytic activity of both the single- and double-wall TiO_2 nanotubes was improved further. *In situ* observations at the annealing temperature of the TiO_2 nanotubes were performed using a transmission electron microscopy (TEM) system. A slower structural failure of the nanotubes was obtained with the introduction of oxygen gas into the TEM column compared with the structural changes observed under high-vacuum conditions without the introduction of oxygen gas. These behaviors suggest that oxygen injection is an important factor in stabilizing the TiO_2 nanotubes during the *in situ* TEM annealing process. The high-magnification TEM images of the double-wall TiO_2 nanotubes revealed that the sintering of the inner wall can draw a clear distinction between the inner and outer walls.

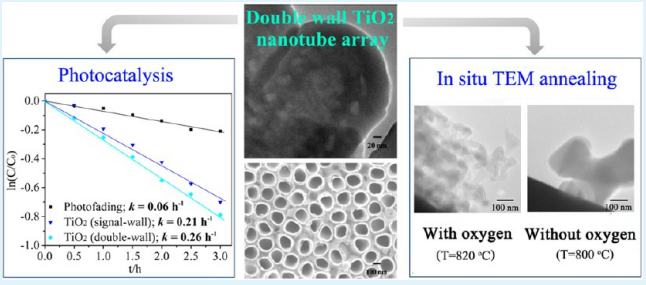

KEYWORDS: *titanium oxide, nanotube, photocatalysis, in situ TEM, self-assembly, anodization*

1. INTRODUCTION

Since the first self-organized anodic oxides of titanium were reported by Zwilling and co-workers in 1999,[1] TiO_2 nanotube arrays with various pore diameters, tube lengths, and specific surface areas have been prepared and investigated in various areas of science.[2] An important improvement in the geometry of TiO_2 nanotubes was reported by Macak et al. and attracted much attention,[3] i.e., TiO_2 nanotubes were synthesized in nonaqueous solutions. The most commonly used nonaqueous electrolytes are glycerol and ethylene glycol.[4] In these organic electrolytes, organic species are decomposed and contaminate the inner part of the tube walls on efficient high-voltage anodization.[5] These new procedures enabled a new research direction: "tube wall design." To date, one of the most important advancements in this topic has been the preparation of TiO_2 nanotube arrays with a double-wall structure. This double-wall nanotube structure has been found to be mechanically robust and maintains its shape during annealing.[6] Based on this finding, more-detailed studies regarding the applications and properties of double-wall TiO_2 nanotube arrays are required.

Among many applications, TiO_2 has been comprehensively studied as a photocatalyst in the past three decades.[7] The photocatalytic performance of TiO_2 nanotubes was also found to be higher than that of the standard P25 nanoparticulate film.[8] Various methods have been examined for further increasing the photocatalytic activity of TiO_2 nanotube arrays. For example, heterostructured TiO_2 nanoparticle−nanotube arrays were prepared as a better photocatalyst, because of their larger surface area.[9,10] The decoration of TiO_2 nanotubes with noble-metal nanoparticles, such as Au,[11] Ag,[12] and Pt,[13] also enhanced their photocatalytic activity. However, almost all these treatments were investigated for single-wall TiO_2 nanotube arrays. Double-wall structures have rarely been investigated as photocatalysis.[14] This led us to exam and study about the photocatalytic activity of double-wall TiO_2 nanotube arrays.

The catalytic behavior of TiO_2 is generally related to its properties (e.g., crystal structure, specific surface area, number of surface −OH groups). With regarding to the detailed investigation on the property of nanostructures, *in situ* transmission electron microscopy (TEM) observations have been widely performed since the 1970s.[15] With this method, samples can be observed with external stresses in TEM equipment in real time. For this reason, *in situ* TEM observations can provides valuable information about morpho-

Received: August 12, 2014
Accepted: November 4, 2014
Published: November 17, 2014

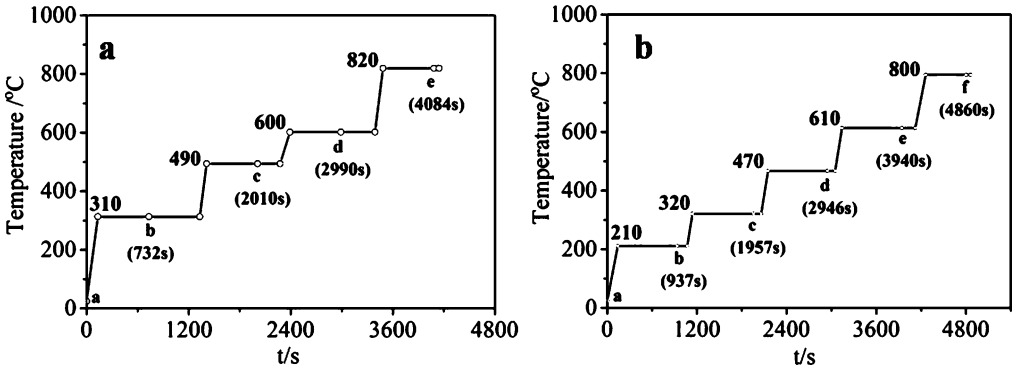

Figure 1. Temperature profiles of the *in situ* TEM annealing experiments (a) with O_2 gas (10^{-4} Pa) and (b) without O_2 gas under high vacuum (2×10^{-5} Pa).

logical changes and properties of double-wall TiO_2 nanotube arrays at various temperatures, which can enhance its application in not only environmental photocatalysis[16] but also biomedical applications,[17] solar energy conversion,[18] and gas sensors.[19]

In this study, double-wall TiO_2 nanotube arrays were prepared by anodization in a glycerol-containing electrolyte. The difference between the photocatalytic activities of the single- and double-wall TiO_2 nanotube arrays is discussed. The decoration of the nanotube arrays with Pt nanoparticles was also performed to improve their photocatalytic activity. Morphological changes during the thermal annealing of the TiO_2 nanotube arrays were observed using an *in situ* TEM heating sample holder.

2. EXPERIMENTAL SECTION

2.1. Preparation of Single- and Double-Wall TiO_2 Nanotube Arrays by Anodization. The detailed procedure has been described in our previous reports.[20,21] Briefly, TiO_2 nanotube arrays were prepared using a conventional two-electrode cell with a direct current power supply (Kikusui, Model KX-100H, Japan). A Ti foil (10 mm × 15 mm, thickness 250 μm, 99.6% purity, Nilaco, Japan) was used as the working electrode (anode). A Pt foil was used as the counter electrode and placed ~3 cm away from the working electrode. The anodization was performed at 60 V for 24 h. In previous reports,[22−24] only ethylene glycol solution was selected to produce double-wall TiO_2 nanotube arrays. In this study, we used glycerol (Junsei Chemical, Japan) as the solvent. NH_4F (Wako Pure Chemical, Japan) and H_2O (purified by Organo/ELGA Purelabo-II, >18 MΩ) were diluted in the glycerol solvent to prepare the electrolyte. Various water contents of the electrolyte were examined to obtain the single- and double-wall TiO_2 nanotube arrays. All resulting samples were washed several times with pure water to completely remove the residual solution and then air-dried. All other chemicals were used as received.

2.2. Characterization of TiO_2 Nanotube Arrays. A JEOL Model JSM-6701F field-emission scanning electron microscopy (FE-SEM) system was used to examine the surface morphology of the obtained nanotube arrays. Films were scraped with a steel blade to observe their side view. The scraped films were also collected on a carbon-coated copper grid for examination via TEM (Hitachi, Model H-9500, 300 kV). X-ray photoelectron spectroscopic (XPS) measurements were performed with an XPS system (JEOL, Model JPS-9200) equipped with a monochromatic Mg Kα source operating at 100 W under ultrahigh vacuum (~1.0×10^{-7} Pa). Binding energies were referenced to the C_{1s} binding energy of the adventitious carbon contamination, which was considered to be 284.8 eV. Atomic ratios of O and Ti in the samples were calculated using peak areas. X-ray diffraction (XRD) patterns were obtained on a Philips X'pert PMD diffractometer with a Panalytical X'celerator detector using Cu Kα radiation, and the scanning speed was 5° min^{-1} at a step of 0.02°. The Brunauer−Emmett−Teller (BET) specific surface area measurement of the annealed single-wall and double-wall TiO_2 nanotubes was carried out on a basis of N_2 adsorption by using Quadrasorb SI (Quantachrome Instruments, USA) instrument. Prior to analyses, TiO_2 nanotubes were scraped from the titanium metal surface, weighed and degassed at 150 °C for 2 h under high vacuum. The values of the specific surface areas (S_{BET}) were determined by using multipoint analysis of adsorption isotherms applying BET equation.

2.3. Decoration of Nanotubes with Pt Nanoparticles. The decoration of Pt nanoparticles on the TiO_2 nanotubes was examined according to a previous report.[25] After calcinations at 450 °C for 3 h under air (Fulltech, Model FT-101FM, Japan; heating rate = 2 °C min^{-1}), the TiO_2 nanotube arrays were transferred into a round-bottom reaction flask filled with 100 mL of an aqueous solution containing 0.01 mM H_2PtCl_6 (Kojima Chemical, Japan) and 0.06 mM NaOH (Kanto, Japan). Subsequently, the flask was maintained at 100 °C in an oil bath for 48 h under air. To obtain metallic Pt nanoparticles on the surface of the TiO_2 nanotubes, the Pt-ion-decorated TiO_2 nanotube arrays were put in a tube furnace (Asone, TMF-500N, Japan) under N_2 and H_2 (1.5 vol %) gas flow at 200 °C for 4 h.

2.4. Photocatalysis Measurements. Samples were cut into pieces with a 1 cm^2 reaction area, and each piece was put into a quartz cell containing 1 ppm Methylene Blue solution (4 mL) and kept in darkness for 40 min to establish the adsorption and desorption equilibrium of Methylene Blue before the tests. A UV lamp (Asone, Model SLUV-4, 9 W, Japan) with a main wavelength of 254 nm was used as a light source. The absorbance of the solutions was measured every 30 min for 3 h with a UV−vis/NIR spectrometer (Perkin−Elmer, Model Lambda 750). The absorption maximum of Methylene Blue showed a peak at 664 nm (see Figure S3 in the Supporting Information).

2.5. TEM Observations and *In Situ* TEM Observations at High Temperature. The detailed nanotube structure was observed using TEM (Hitachi, Model H-9500, 300 kV). The annealing behavior of the double-wall TiO_2 nanotubes was observed in the same TEM system with a filament-type specimen heating holder.[26] The sample nanotubes were put on a Pt (70%)−Ir (30%) filament (see Figure S1 in the Supporting Information), and the specimen behavior was recorded on an AMT CCD camera with an NTST frame rate of 29.97 fps. The filament temperature was controlled by the current value, which was calibrated by the melting points of known metals, such as Ag and Sb. *In situ* observations were performed under high vacuum (~2×10^{-5} Pa) and oxygen atmosphere (10^{-4} Pa oxygen). The temperature profiles of these *in situ* TEM annealing experiments are shown in Figure 1. Several still high-resolution images were also captured.

3. RESULTS AND DISCUSSION

3.1. Preparation of Single- and Double-Wall TiO_2 Nanotube Arrays by Anodization. Figure 2 shows the

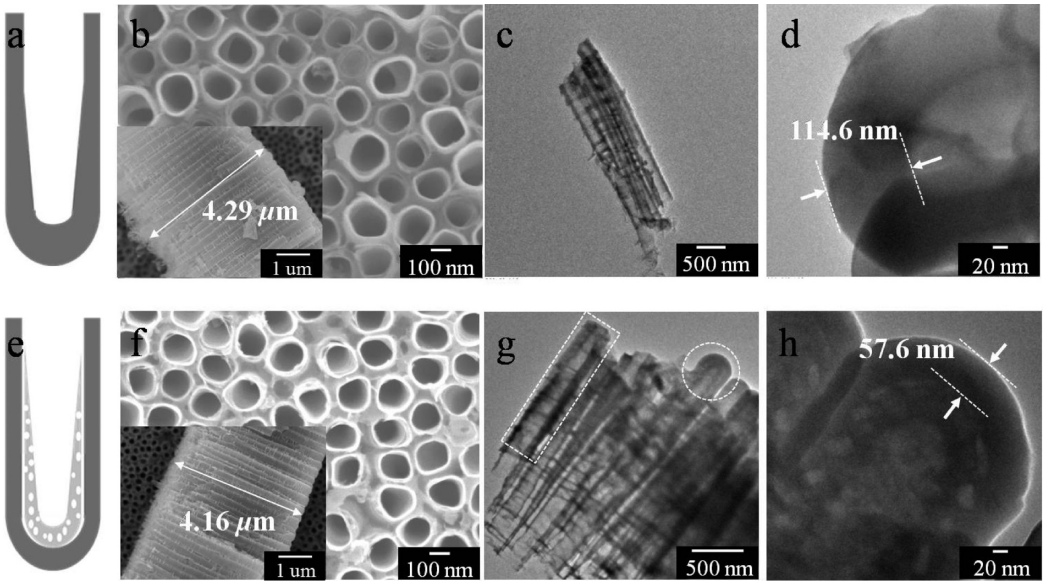

Figure 2. (a,e) Schematic illustrations, (b, f) SEM images, and (c, d, g, h) TEM images of ((a–d) single-wall and (e–h) double-wall TiO_2 nanotube arrays prepared by anodization in electrolyte (single-wall nanotubes: 91.5 wt % glycerol + 8 wt % H_2O + 0.5 wt % NH_4F; double-wall nanotubes: 96.5 wt % glycerol + 3 wt % H_2O + 0.5 wt % NH_4F).

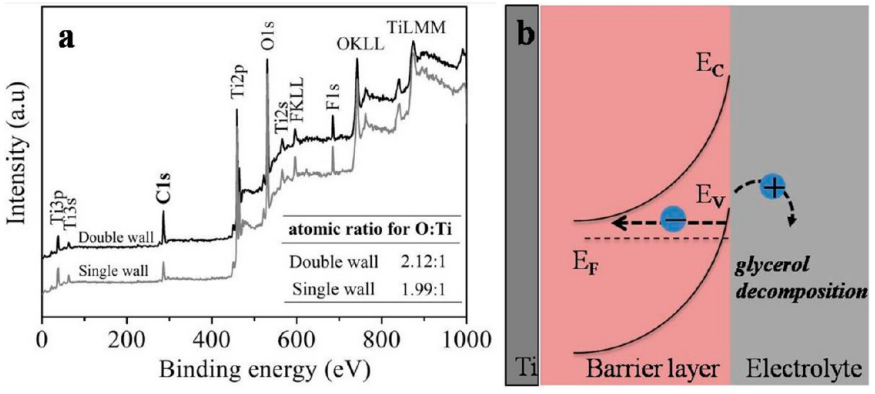

Figure 3. (a) Wide-scan XPS profile of single- and double-wall TiO_2 nanotube arrays prepared by anodization in electrolyte (single-wall nanotube: 91.5 wt % glycerol + 8 wt % H_2O + 0.5 wt % NH_4F; double-wall: 96.5 wt % glycerol + 3 wt % H_2O + 0.5 wt % NH_4F). Inset shows atomic ratios for O:Ti of single- and double-wall TiO_2 nanotube arrays; (b) schematic illustration of the tunneling or avalanche breakdown of the Schottky barrier, which induces the glycerol decomposition under low water content (E_C = conductive band energy; E_F = Fermi energy; E_V = valence band energy).

SEM and TEM images of two typical as-prepared TiO_2 nanotube arrays. From the SEM images, Figures 2b and 2f show films only with a single-wall structure on the surface, and the film thicknesses are ~4.3 μm and ~4.2 μm, respectively. In Figure 2g, the double-wall structure can be observed at the root segment of the nanotube (dashed circle), and an inner wall was enclosed inside the outer wall (see Figure 2h). However, this double-wall structure cannot be observed in Figure 2c, and the bottom of the nanotube shows only a dense tube wall, which is a single-wall structure (see Figure 2d). Thus, a transition from a single-wall construct to a double-wall construct was achieved by decreasing the water content of the electrolyte, from 8 wt % to 3 wt %. This was presumably due to the excessive etching of the tube mouth,[27] TiO_2 nanotubes showing a conelike structure (highlighted rectangular feature in Figure 2g), and double-wall existing only at the root segment of the tube.

Similar to a previous report,[6] our double-wall TiO_2 nanotubes also suffered carbon contamination in the inner wall. As shown in the XPS spectra in Figure 3a, the double-wall TiO_2 nanotube arrays showed a higher carbon peak than the single-wall TiO_2 nanotube arrays. For preparation of the single- and double-wall structures, only the water contents of the electrolytes used for the preparation were different. Thus, a double-wall structure with a higher carbon contamination was observed in the nanotube arrays prepared under a lower water content. The formation of higher carbon contamination in the inner wall is probably due to the *IR*-drop effects; that is, the effective voltage of the electrode is given as $U_{eff} = U_{nominal} - IR$, where R is the resistivity of the electrolyte, and I is the current.[28] During the anodization process, the viscosity of glycerol aqueous solution decreases due to the addition of water.[29] Electrolytes with lower water content have higher viscosity, according to the following Stokes–Einstein relationship:

$$D = \frac{k_B T}{6\pi\eta a} \quad (1)$$

where D is the diffusion constant, T the absolute temperature, η the dynamic viscosity, k_B the Boltzmann's constant, and a the

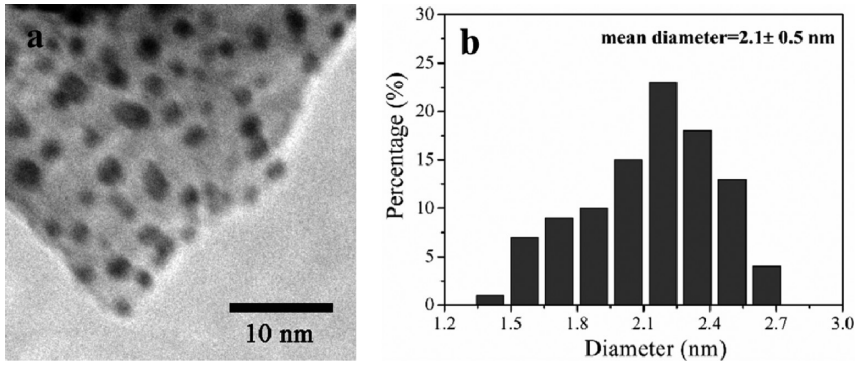

Figure 4. (a) TEM image of Pt nanoparticles decorated on double-wall TiO_2 nanotube arrays. (b) Size distribution of the decorated Pt nanoparticles. The mean diameter of Pt nanoparticles was ~2.1 nm.

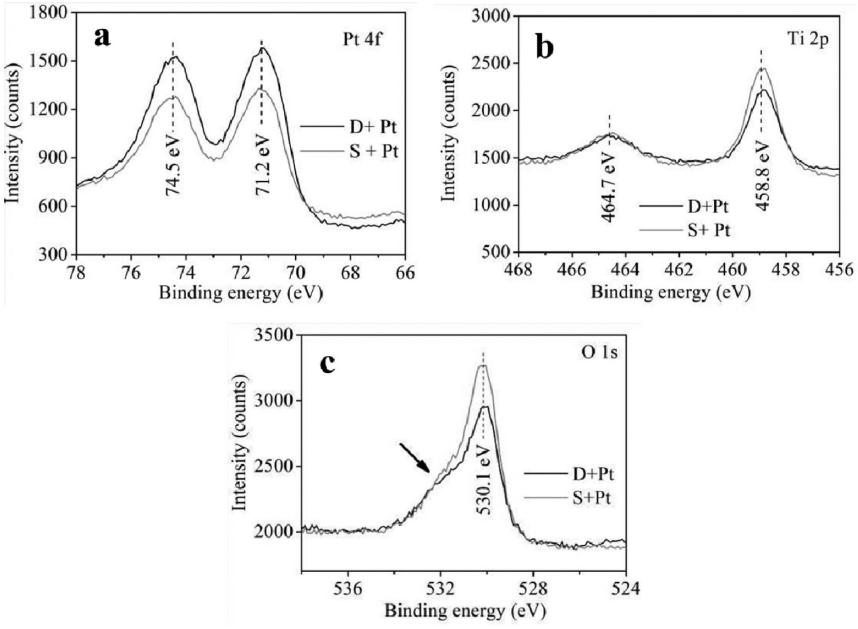

Figure 5. XPS spectra of single- and double-wall TiO_2 nanotube arrays decorated with Pt nanoparticles. (a) Pt_{4f} spectra, (b) Ti_{2p} spectra, and (c) O_{1s} spectra. S + Pt: single-wall TiO_2 nanotube arrays with Pt decoration; D + Pt: double-wall TiO_2 nanotube arrays with Pt decoration.

radius of ions. The diffusion rate of species inside the electrolyte is slow under a high viscosity condition, conductivity of the electrolyte should be very low. So the *IR*-drop effects on the structure of the anodized TiO_2 nanotube arrays should be considered.

In our experiment, according to the decrease of water content from 8 wt % to 3 wt %, fluoride ions or water molecules may be decreased by the growth of anodic film in the electrolyte near barrier layer. Thus, a significant *IR*-drop effect will cause a thinner barrier layer.[30] This is confirmed in the insets of Figures 2c and 2f. The thickness of the barrier layer is ~57.6 nm for the double-wall nanotube, which is almost half that of the single-wall structure (114.6 nm). Such a thin barrier layer of double-wall nanotube will produce a high electrical field under an anodization voltage of 60 V, and the tunneling in the Schottky barrier generates holes (Figure 3b).[31] The generated holes decompose glycerol, and the decomposed products (e.g., glyceric acid, glycolaldehyde, and glycolic acid) possibly react with Ti^{4+} at the electrolyte−TiO_2 interface to form the inner wall of the double-wall nanotube, resulting in carbon contamination.[32,33] This reaction induces a higher amount of oxygen inside the TiO_2 nanotube arrays. Compared with stoichiometric TiO_2, the double-wall TiO_2 nanotube arrays show a relatively higher O:Ti atomic ratio of 2.12:1 (see Figure 3a). On the other hand, under a water content of 8 wt %, the thicker barrier layer (d = 114.6 nm) produces the lower electric field; thus, the hole generation should be difficult, because of the inefficient tunneling. In this case, decomposition of glycerol is quite difficult, and the resulting TiO_2 nanotube contains a low carbon content and has a dense single-wall structure. Therefore, the inner wall of the double-wall TiO_2 nanotubes was obtained because of the decomposition of glycerol in the thin barrier layer.

3.2. Pt Decoration of Single- and Double-Wall TiO_2 Nanotube Arrays and Their Photocatalytic Activity. For the modification of the TiO_2 nanotubes with Pt nanoparticles, a deposition−precipitation method was examined.[25] The TEM photograph in Figure 4a shows uniformly dispersed Pt deposits on the TiO_2 surface. The average diameter of the Pt deposits was ~2.1 nm (see Figure 4b). Because of the small particle size, the TiO_2 nanotube array structure was well maintained (see Figures S2a and S2b in the Supporting Information). Tube blockage with Pt was not observed. The TEM images in Figures S2c and S2d in the Supporting Information show that both the

single-wall and double-wall structures were not destroyed after Pt deposition.

After thermal treating with N_2 and H_2 gases at 200 °C for 4 h, the Pt deposits were reduced to metallic Pt nanoparticles. As shown in Figure 5a, the signals for Pt $4f_{7/2}$ and Pt $4f_{5/2}$ were located at 71.2 and 74.5 eV, respectively, and the spin splitting matched well with the standard data of Pt^0 (3.3 eV).[13] Figure 5b shows that Ti $2p_{3/2}$ and Ti $2p_{1/2}$ were located at 458.8 and 464.7 eV, respectively. These values were similar to that of TiO_2, suggesting that Ti was in the +4 oxidation state and directly bonded to oxygen.[34] As shown in Figure 5c, the asymmetric spectrum of O_{1s} indicated the presence of at least two chemical conditions of oxygen. The dominant peak at 530.1 eV was from the titania lattice.[35] Another tailing peak, indicated by the black arrow, can be attributed to the surface hydroxyl groups.[34] Hydroxyl groups may locate on the surface of the deposited Pt nanoparticles. Pt deposition was reported to significantly improve the capture ability of the hydroxyl groups.[36,37]

Figure 6 illustrates the photocatalytic activity of the single- and double-wall TiO_2 nanotube arrays before and after Pt decoration. Without the TiO_2 nanotube arrays, almost no degradation of Methylene Blue was observed under the irradiation conditions. With the TiO_2 nanotube arrays, the maximum absorption peak of Methylene Blue at 664 nm clearly decreased with increasing UV irradiation time by the photocatalytic activity of the TiO_2 nanotubes (see Figure S3 in the Supporting Information). The degradation of Methylene Blue can be analyzed by first-order kinetics, with the classical equation of $\ln(C/C_0) = kt$, where k is the rate constant and t is the time.[38] By comparing the rate constants shown in Figure 6, the double-wall TiO_2 nanotube arrays were observed to exhibit better photocatalytic activity than the single-wall TiO_2 nanotube arrays. With regard to this enhanced photocatalytic activity of double-wall TiO_2 nanotube arrays, XPS, XRD, SEM, and specific surface area of the annealed single- and double-wall TiO_2 nanotube arrays were further characterized. After annealing, the XPS spectra (Figure S4a in the Supporting Information) indicates almost same chemical composition in single-wall and double-wall TiO_2 nanotube arrays, thus the carbon impurities in double-wall TiO_2 nanotube arrays could be released during annealing. The XRD patterns for both annealed single- and double-wall TiO_2 nanotube arrays also show identical peak positions and the presence of anatase phase (see Figure S4b in the Supporting Information). However, in Figures S4c and S4d in the Supporting Information, different from the single-wall TiO_2 nanotube, the tube wall of double-wall TiO_2 nanotube split into two layers, and the inner wall exhibited a loose and porous structure (Figures S4c and S5c in the Supporting Information). These morphological details contribute to a larger surface area of the double-wall TiO_2 nanotube arrays. BET analysis further confirmed the enlarged surface area of the annealed double-wall TiO_2 nanotube arrays. The specific surface area of the annealed double-wall TiO_2 nanotube was 26.11 m^2/g, while that of annealed single-wall TiO_2 nanotube was 17.67 m^2/g. Therefore, we concluded that the enlarged surface area of double-wall TiO_2 nanotube array should be the main reason for its improved photocatalytic activity. Moreover, the specific surface area is also the most important factor in determining the amount of Pt particles on the surface.[25] As shown in Figure 5a, a higher peak intensity of Pt was observed in the double-wall structure, indicating that this structure supports a larger amount of Pt nanoparticles than the single-wall structure.

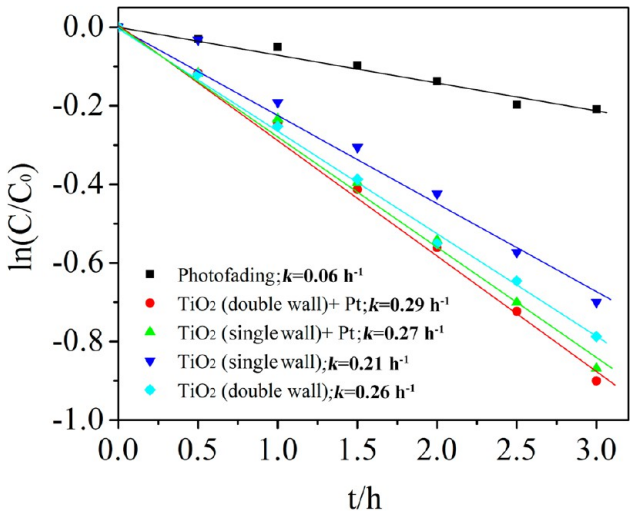

Figure 6. Photocatalytic degradation rates of Methylene Blue in the presence of the annealed single- and double-wall TiO_2 nanotube arrays before and after Pt decoration (single-wall nanotube: 91.5 wt % glycerol + 8 wt % H_2O + 0.5 wt % NH_4F; 60 V, 24 h; double-wall nanotube: 96.5 wt % glycerol + 3 wt % H_2O + 0.5 wt % NH_4F; 60 V, 24 h).

Regarding the decoration of Pt nanoparticles, the work function of Pt (ϕ_m = 4.98−5.7 eV) is higher than TiO_2 ($\phi_m \approx$ 4.6 eV), thus the photogenerated electrons will transfer from TiO_2 to Pt.[39] A Schottky barrier, which features a higher potential gradient, will form at the Pt/TiO_2 interface. The Schottky barrier can retard the electron−hole recombination process.[40] Therefore, the decoration of Pt nanoparticles could enhance the generation of photoelectron−hole pairs and achieve a higher photocatalytic activity. Moreover, an obvious amount of hydroxyl groups was confirmed in XPS (Figure 5c). Because the photocatalytic degradation of Methylene Blue is mainly initiated by •OH,[41] this high content of surface hydroxyl groups could facilitate the photocatalytic reactions, as the −OH groups can easily capture photoinduced holes to produce •OH free radicals. Thus, as shown in Figure 6, compared with the bare samples, the photocatalytic activity was further enhanced by Pt decoration for both the single- and double-wall TiO_2 nanotube arrays.

3.3. High-Temperature *In Situ* TEM Observations of Double-Wall TiO_2 Nanotube Arrays. Except for the improved photocatalytic activities due to the enhanced specific surface area of double-wall structure, the crystalline behavior of TiO_2 nanotube arrays also can improve the photoelectric properties.[42] However, research on this topic has been mostly based on *ex situ* annealing methods.[43,44] Conversely, *in situ* TEM observation at high temperature is a unique and powerful technique to observe the calcination and sintering processes during heating in real time. Recently, we have succeeded to observe the structure changes of copper and other fine particles and nanoparticles at high temperature by using this method.[45−48] With this system, gases can be introduced into the TEM column.

Here, *in situ* TEM observations of the double-wall TiO_2 nanotube arrays were performed at various temperatures under the introduction of oxygen gas.[21] Figure 7 shows the morphological changes of the nanotubes. Before the *in situ*

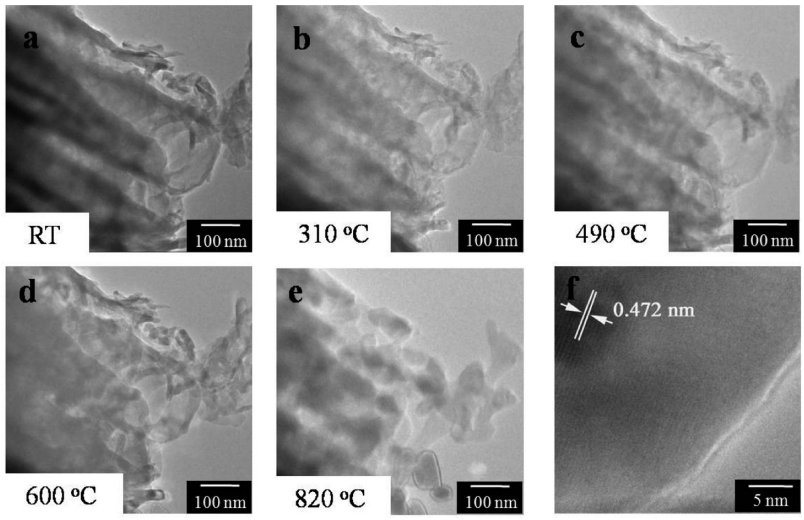

Figure 7. (a–e) TEM images of double-wall TiO_2 nanotube arrays at various temperatures with the introduction of oxygen gas (all images were collected at the points marked in Figure 1a; RT = room temperature). (f) A high-resolution TEM image of a double-wall TiO_2 nanotube wall at 820 °C.

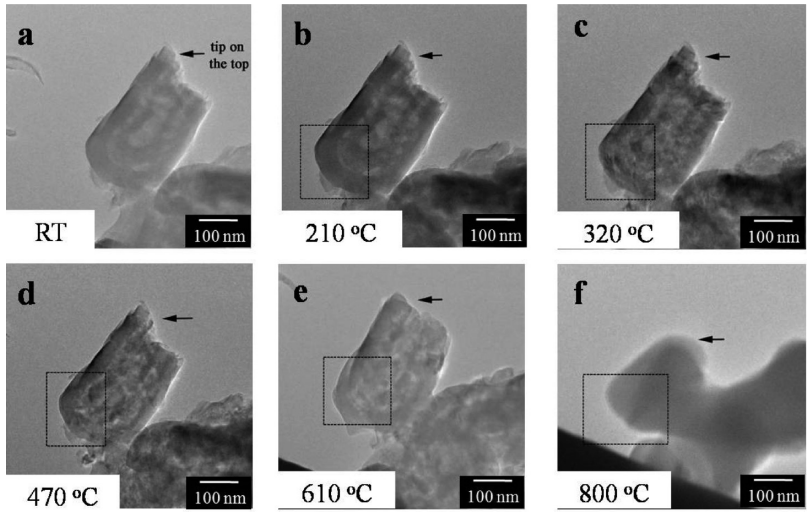

Figure 8. (a–f) Low magnification TEM images of double-wall TiO_2 nanotubes at various temperatures without the introduction of oxygen gas (all images were collected at the points marked in Figure 1b).

TEM annealing, a nanotube structure could be observed (Figure 7a). In the temperature range of 310–600 °C, the crystallization of TiO_2 nanotubes caused a sharp contrast in the TEM images (Figures 7b, 7c, and 7d),[49] but the structural failure of the nanotubes was not observed. Many protruding ends still existed after heating at 600 °C for ca. 10 min (Figure 7d), but the nanotube did not collapse. At 820 °C, a structural failure of the nanotubes was observed after keeping the sample at this temperature for ca. 10 min. The nanotube collapsed and transformed into a coral structure that contained many intercolumnar pores (Figure 7e). The coalescence of crystal grains and sintering are probably responsible for this structural transformation.

The *in situ* TEM observations of the annealing of the double-wall TiO_2 nanotubes were also performed without the introduction of oxygen gas. A different behavior was observed compared with that under the introduction of oxygen gas. As shown in Figure 8, the nanotubes were not stable, even at 610 °C. As shown in Figure 8e, a tip on the top of the tube (denoted by the black arrow) disappeared after annealing at 610 °C for ca. 10 min, and the failure of the tubes was obvious. At 800 °C, the structural failure proceeded dramatically, the nanotubes completely collapsed after annealing for ca. 10 min, and they formed a stonelike structure (Figure 8f). This stonelike structure was highly different from the final coral structure obtained under oxygen gas. Therefore, during the *in situ* TEM annealing process, the nanotube was less stable under high-vacuum conditions than that obtained in the presence of oxygen, and the sintering of the TiO_2 nanotubes was accelerated under high-vacuum conditions. Moreover, at 610 °C, the sintering of the inner wall also optimized the double-wall structure, and the inner and outer walls were clearly separated from each other (see Figure S5d in the Supporting Information).

A high-resolution TEM image was also captured after annealing at 820 °C for ca. 10 min in the presence of oxygen gas and is displayed in Figure 7f. The image shows lattice fringes (0.472 nm) similar to the lattice spacing of γ-Ti_3O_5 (002) (0.469 nm).[50] Under oxidizing conditions, such as in the presence of air and oxygen, amorphous TiO_2 nanotube arrays

are converted to the crystalline phase at high temperature. Suboxide phases of TiO_2 are usually difficult to detect.[51] The emergence of γ-Ti_3O_5 in this study indicated that oxygen defects were generated in the TiO_2 nanotubes under reduced pressure (10^{-3} Pa) at high temperature, even in the presence of oxygen gas.

TiO_2 is reported to decompose at high temperatures and low oxygen pressures.[52] Similarly, under the high-vacuum conditions of TEM without the introduction of oxygen gas, the decomposition of the TiO_2 nanotubes occurred reasonably during the *in situ* TEM annealing process. In our primary communication, we reported that the lattice fringe of TiO_2 crystals can be found at 320 °C (see Figure S6 in the Supporting Information). Oxygen molecules adsorbed on anatase TiO_2 will desorb at ∼140 °C under high-vacuum conditions;[53] thus, oxygen vacancy cannot be excluded, because of the loss of oxygen during the *in situ* TEM annealing of the TiO_2 nanotubes without the introduction of oxygen.

By comparing Figures 7 and 8, we can conclude that a higher morphological stability of the TiO_2 nanotubes at high temperature was obtained in the presence of oxygen gas in the TEM column. For the sintering of TiO_2, oxygen ion diffusion was considered to be the rate-determining step.[54] From the above discussion, oxygen defects exist for the *in situ* TEM annealing of TiO_2, and these defects tend to favor the diffusion and accelerate the sintering of TiO_2. As shown in Figure 7, exposure to a high dose of oxygen can heal oxygen vacancies,[55] and it is reasonable for a low concentration of oxygen vacancies to occur. This would tend to slow the sintering of TiO_2 and stabilize the TiO_2 nanotubes during the *in situ* TEM annealing process.

From these *in situ* TEM observations of the annealing of the TiO_2 nanotubes, it can be concluded that oxygen gas molecules can stabilize the structures. The details of the *in situ* TEM annealing of the TiO_2 nanotubes need further research. The anatase−rutile phase transition of TiO_2 has been reported to be affected by the concentration of oxygen vacancies.[56,57] During the *in situ* TEM annealing of the TiO_2 nanotube, the oxygen pressure may also affect the phase transition of the TiO_2 nanotube.

4. CONCLUSION

In summary, the TiO_2 nanotube arrays were prepared by anodization in glycerol−water electrolytes. A decrease of water content in the electrolyte changed the resulting tube structure from single-wall to double-wall. The double-wall TiO_2 nanotube arrays exhibited better photocatalytic activity than the single-wall nanotube arrays. This enhancement was mainly due to a larger surface area of the double-wall structures. After Pt decoration, the photocatalytic activity of both the structures was further improved. The *in situ* TEM observations of the TiO_2 nanotubes at high temperatures were also investigated. In the presence of oxygen gas, the sintering of the TiO_2 nanotubes was slow, but a clear tube failure into a coral structure was observed at 820 °C. In contrast, a faster sintering of the nanotubes was observed under high vacuum. This indicated a dependence of the morphological changes of the TiO_2 nanotubes on the gas atmosphere during the *in situ* annealing process, and it also indicated that oxygen can stabilize the TiO_2 nanotubes.

■ ASSOCIATED CONTENT

Ⓢ Supporting Information

Detailed information on experiments and some supporting SEM and TEM images are collected in Supporting Information. This material is available free of charge via the Internet at http://pubs.acs.org.

■ AUTHOR INFORMATION

Corresponding Author

*Fax: +81-11-706-7110. E-mail: tetsu@eng.hokudai.ac.jp.

Present Address

[§]Graduate School of Urban Environmental Sciences, Tokyo Metropolitan University, Minami-ohsawa 1-1, Hachioji, Tokyo, 192-0397, Japan.

Funding

This work is partially supported by Hokkaido University and Grant-in-Aid for Scientific Research in Priority Area "New Polymeric Materials Based on Element-Blocks (2401)" (No. 25102501).

Notes

The authors declare no competing financial interest.

■ ACKNOWLEDGMENTS

Authors thank Professor B. Ohtani and Dr. M. Takase (Hokkaido University) for kind experimental assistance of BET specific surface area measurement.

■ REFERENCES

(1) Zwilling, V.; Darque-Ceretti, E.; Boutry-Forveille, A.; David, D.; Periin, M. Y.; Aucouturier, M. Structure and Physicochemistry of Anodic Oxide Films on Titanium and TA6V Alloy. *Surf. Interface Anal.* **1999**, *27*, 629−637.

(2) Alub, S. P.; Roy, P.; Virtanen, S.; Schmuki, P. Self-Organized TiO_2 Nanotube Arrays: Critical Effects on Morphology and Growth. *Isr. J. Chem.* **2010**, *50*, 453−467.

(3) Macak, J. M.; Tsuchiya, H.; Ghicov, A.; Schmuki, P. Dye-Sensitized Anodic TiO_2 Nanotubes. *Electrochem. Commun.* **2005**, *7*, 1133−1137.

(4) Liu, R.; Yang, W. D.; Qiang, L. S.; Wu, J. F. Fabrication of TiO_2 Nanotube Arrays by Electrochemical Anodization in an NH_4F/H_3PO_4 Electrolyte. *Thin Solid Films* **2011**, *519*, 6459−6466.

(5) Albu, S. P.; Schmuki, P. TiO_2 Nanotubes Grown in Different Organic Electrolytes: Two-Size Self-Organization, Single vs. Double-Walled Tubes, and Giant Diameters. *Phys. Status Solidi RRL* **2010**, *4*, 215−217.

(6) Albu, S. P.; Ghicov, A.; Aldabergenova, A.; Drechsel, P.; LeClere, D.; Thompson, G. E.; Macak, J. M.; Schmuki, P. Formation of Double-Walled TiO_2 Nanotubes and Robust Anatase Membranes. *Adv. Mater.* **2008**, *20*, 4135−4139.

(7) Hashimoto, K.; Irie, H.; Fujishima, A. TiO_2 Photocatalysis: A Historical Overview and Future Prospects. *Jpn. J. Appl. Phys.* **2005**, *44*, 8269−8285.

(8) Liu, Z. Y.; Zhang, X. T.; Nishimoto, S.; Murakami, T.; Fujishima, A. Efficient Photocatalytic Degradation of Gaseous Acetaldehyde by Highly Ordered TiO_2 Nanotube Arrays. *Environ. Sci. Technol.* **2008**, *42*, 8547−8551.

(9) Huo, K. F.; Wang, H. R.; Zhang, X. M.; Cao, Y.; Chu, P. K. Heterostructured TiO_2 Nanoparticles/Nanotube Arrays: In Situ Formation from Amorphous TiO_2 Nanotube Arrays in Water and Enhanced Photocatalytic Activity. *ChemPlusChem* **2012**, *77*, 323−329.

(10) Chu, F.; Li, W.; Shi, C. S.; Liu, E. Z.; He, C. N.; Li, J. J.; Zhao, N. Q. Performance Improvement of Dye-Sensitized Solar Cells Using Room-Temperature-Synthesized Hierarchical TiO_2 Honeycomb Nanostructures. *ACS Appl. Mater. Interfaces* **2013**, *5*, 7170−7175.

(11) Hosseini, M. G.; Faraji, M.; Momeni, M. M. Application of Titanium Oxide Nanotube Films Containing Gold Nanoparticles for the Electroanalytical Determination of Ascorbic Acid. *Thin Solid Films* **2011**, *519*, 3457−3461.
(12) He, X. L.; Cai, Y. Y.; Zhang, H. M.; Liang, C. H. Photocatalytic Degradation of Organic Pollutants with Ag Decorated Free-Standing TiO_2 Nanotube Arrays and Interface Electrochemical Response. *J. Mater. Chem.* **2011**, *21*, 475−480.
(13) Rettew, R. E.; Allam, N. K.; Alamgir, F. M. Interface Architecture Determined Electrocatalytic Activity of Pt on Vertically Oriented TiO_2 Nanotubes. *ACS Appl. Mater. Interfaces* **2011**, *3*, 147−151.
(14) Paramasivam, I.; Jha, H.; Liu, N.; Schmuki, P. A Review of Photocatalysis Using Self-organized TiO_2 Nanotubes and Other Ordered Oxide Nanostructures. *Small* **2012**, *8*, 3073−3103.
(15) Yoshida, K.; Yamasaki, J.; Tanaka, N. *In Situ* High-Resolution Transmission Electron Microscopy Observation of Photodecomposition Process of Poly-hydrocarbons on Catalytic TiO_2 Films. *Appl. Phys. Lett.* **2004**, *84*, 2542−2544.
(16) Wender, H.; Feil, A. F.; Diaza, L. B.; Ribeiro, C. S.; Machado, G. J.; Migowski, P.; Weibel, D. E.; Dupont, J.; Teixeira, S. R. Self-Organized TiO_2 Nanotube Arrays: Synthesis by Anodization in an Ionic Liquid and Assessment of Photocatalytic Properties. *ACS Appl. Mater. Interfaces* **2011**, *3*, 1359−1365.
(17) Jeong, Y. H.; Lee, K.; Choe, H. C.; Ko, Y. M.; Brantley, W. A. Nanotube Formation and Morphology Change of Ti Alloys Containing Hf for Dental Materials Use. *Thin Solid Films* **2009**, *517*, 5365−5369.
(18) Wang, X. Y.; Sun, L. D.; Zhang, S.; Wang, X. Ultralong, Small-Diameter TiO_2 Nanotubes Achieved by an Optimized Two-Step Anodization for Efficient Dye-Sensitized Solar Cells. *ACS Appl. Mater. Interfaces* **2014**, *6*, 1361−1365.
(19) Yongseok, J.; Park, J. H.; Kang, M. G. The Preparation of Highly Ordered TiO_2 Nanotube Arrays by an Anodization Method and Their Applications. *Chem. Commun.* **2012**, *48*, 6456−6471.
(20) Xue, C. R.; Narushima, T.; Yonezawa, T. Direct SEM Observation of Non-Electroconductive $TiOF_2$ Nanotube Arrays Prepared by Anodization Using an Ionic Liquid as a Visualizing Reagent. *J. Inorg. Organomet. Polym. Mater.* **2013**, *23*, 239−242.
(21) Xue, C. R.; Narushima, T.; Ishida, Y.; Tokunaga, T.; Yonezawa, T. *In Situ* TEM Observation of Double-Wall TiO_2 Nanotube Arrays at High Temperature. *Chem. Lett.* **2014**, *43*, 1514−1516.
(22) Ji, Y. J.; Lin, K. C.; Zheng, H. G.; Zhu, J. J.; S. Samia, A. C. Fabrication of Double-walled TiO_2 Nanotubes with Bamboo Morphology via One-step Alternating Voltage Anodization. *Electrochem. Commun.* **2011**, *13*, 1013−1015.
(23) Wu, H. J.; Zhang, Z. H. High Photoelectrochemical Water Splitting Performance on Nitrogen Doped Double-wall TiO_2 Nanotube Array Electrodes. *Int. J. Hydrogen Energy* **2011**, *36*, 13481−13487.
(24) Ni, J. H.; Noh, K.; Frandsen, C. J.; Kong, S. D.; He, G.; Tang, T. T.; Jin, S. Preparation of Near Micrometer-Sized TiO_2 Nanotube Arrays by High Voltage Anodization. *Mater. Sci. Eng., C* **2013**, *33*, 259−264.
(25) Sunagawa, Y.; Yamamoto, K.; Takahashi, H.; Muramatsu, A. Liquid-Phase Reductive Deposition as a Novel Nanoparticle Synthesis Method and Its Application to Supported Noble Metal Catalyst Preparation. *Catal. Today* **2008**, *132*, 81−87.
(26) Narushima, T.; Tsukamoto, H.; Yonezawa, T. High Temperature Oxidation Event of Gelatin Nanoskin-Coated Copper Fine Particles Observed by *In Situ* TEM. *AIP Adv.* **2012**, *2*, 042113.
(27) Song, Y. Y.; Lynch, R.; Kim, D.; Roy, P.; Schmuki, P. TiO_2 Nanotubes: Efficient Suppression of Top Etching during Anodic Growth. *Electrochem. Solid-State Lett.* **2009**, *12*, C17−C20.
(28) Roy, P.; Berger, S.; Schmuki, P. TiO_2 Nanotubes: Synthesis and Applications. *Angew. Chem., Int. Ed.* **2011**, *50*, 2904−2939.
(29) Segur, J. B.; Obstar, H. E. Viscosity of Glycerol and Its Aqueous Solutions. *Ind. Eng. Chem.* **1951**, *43*, 2117−2120.
(30) Valota, A.; LeClere, D. J.; Skeldon, P.; Curioni, M.; Hashimoto, T.; Berger, S.; Kunze, J.; Schmuki, P.; Thompson, G. E. Influence of Water Content on Nanotubular Anodic Titania Formed in Fluoride/Glycerol Electrolytes. *Electrochim. Acta* **2009**, *54*, 4321−4327.
(31) Song, Y. Y.; Roy, P.; Paramasivam, I.; Schmuki, P. Voltage-Induced Payload Release and Wettability Control on TiO_2 Nanotubes. *Angew. Chem.* **2010**, *122*, 361−364.
(32) Okada, K. *Electrochemical Oxidation of Glycerol in a Proton-Exchange-Membrane Reactor*. Ph.D. Thesis, The University of Michigan, Ann Arbor, MI, USA, 2013.
(33) Liu, N.; Mirabolghasemi, H.; Lee, K.; Albu, S. P.; Tighineanu, A.; Altomare, M.; Schmuki, P. Anodic TiO_2 Nanotubes: Double Walled vs. Single Walled. *Faraday Discuss.* **2013**, *164*, 107−116.
(34) Smith, Y. R.; Sarma, B.; Mohanty, S. K.; Misra, M. Light-Assisted Anodized TiO_2 Nanotube Arrays. *ACS Appl. Mater. Interfaces* **2012**, *4*, 5883−5890.
(35) Xu, Q. F.; Liu, Y.; Lin, F. J.; Mondal, B.; Lyons, A. M. Superhydrophobic TiO_2−Polymer Nanocomposite Surface with UV-Induced Reversible Wettability and Self-Cleaning Properties. *ACS Appl. Mater. Interfaces* **2013**, *5*, 8915−8924.
(36) Zhang, J.; Li, L. P.; Yan, T. J.; Li, G. S. Selective Pt Deposition onto the Face (110) of TiO_2 Assembled Microspheres that Substantially Enhances the Photocatalytic Properties. *J. Phys. Chem. C* **2011**, *115*, 13820−13828.
(37) Jing, L. Q.; Wang, D. J.; Wang, B. Q.; Li, S. D.; Xin, B. F.; Fu, H. G.; Sun, J. Z. Effects of Noble Metal Modification on Surface Oxygen Composition, Charge Separation and Photocatalytic Activity of ZnO Nanoparticles. *J. Mol. Catal. A: Chem.* **2006**, *244*, 193−200.
(38) Xiao, F. X. Self-Assembly Preparation of Gold Nanoparticles-TiO_2 Nanotube Arrays Binary Hybrid Nanocomposites for Photocatalytic Applications. *J. Mater. Chem.* **2012**, *22*, 7819−7830.
(39) Schubert, G.; Bánsági, T.; Solymosi, F. Photocatalytic Decomposition of Methyl Formate over TiO_2-Supported Pt Metals. *J. Phys. Chem. C* **2013**, *117*, 22797−22804.
(40) Zhou, W. J.; Guan, Y.; Wang, D. Z.; Zhang, X. H.; Liu, D.; Jiang, H. D.; Wang, J. Y.; Liu, X. G.; Liu, H.; Chen, S. W. PdO/TiO_2 and Pd/TiO_2 Heterostructured Nanobelts with Enhanced Photocatalytic Activity. *Chem. Asian J.* **2014**, *9*, 1648−1654.
(41) Xie, Y.; Ali, G.; Yoo, S. H.; Cho, S. O. Sonication-Assisted Synthesis of CdS Quantum-Dot-Sensitized TiO_2 Nanotube Arrays with Enhanced Photoelectrochemical and Photocatalytic Activity. *ACS Appl. Mater. Interfaces* **2010**, *2*, 2910−2914.
(42) Lee, S.; Park, I. J.; Kim, D. H.; Seong, W. M.; Kim, D. W.; Han, G. S.; Kim, J. Y.; Jung, H. S.; Hong, K. S. Crystallogrphically Preferred Oriented TiO_2 Nanotube Arrays for Efficient Photovoltaic Energy Conversion. *Energy Environ. Sci.* **2012**, *5*, 7989−7995.
(43) Albu, S. P.; Tsuchiya, H.; Fujimoto, S.; Schmuki, P. TiO_2 Nanotubes-Annealing Effects on Detailed Morphology and Structure. *Eur. J. Inorg. Chem.* **2010**, 4351−4356.
(44) Lin, J.; Guo, M.; Y, C. T.; Lu, W.; Zhang, G. G.; Liu, X. L.; Zhou, L. M.; Chen, X. F.; Huang, H. T. High Temperature Crystallization of Free-Standing Anatase TiO_2 Nanotube Membranes for High Efficiency Dye-Sensitized Solar Cells. *Adv. Funct. Mater.* **2013**, *23*, 5952−5960.
(45) Narushima, T.; Hyono, A.; Nishida, N.; Yonezawa, T. *In-Situ* Heating TEM Observation of Microscopic Structural Changes of Size-Controlled Metallic Copper/Gelatin Composite. *J. Nanosci. Nanotechnol.* **2012**, *12*, 7764−7776.
(46) Ida, K.; Tomonari, M.; Sugiyama, Y.; Chujyo, Y.; Tokunaga, T.; Yonezawa, T.; Kuroda, K.; Sasaki, K. Behavior of Cu Nanoparticles Ink under Reductive Calcination for Fabrication of Cu Conductive Film. *Thin Solid Films* **2012**, *520*, 2789−2793.
(47) Narushima, T.; Lu, R.; Yonezawa, T. Wet Preparation of Organic-Stabilizer-Free Urchin Structured Nickel Fine Particles and Their *In situ* TEM Observation at High Tempeartures. *Mater. Trans.* **2014**, *55*, 1474−1478.
(48) Yonezawa, T.; Arai, S.; Takeuchi, H.; Kamino, T.; Kuroda, K. Preparation of Naked Silver Nanoparticles in a TEM Column and Direct *In Situ* Observation of Their Structural Changes at High Temperature. *Chem. Phys. Lett.* **2012**, *537*, 65−68.

(49) Fang, D.; Luo, Z. P.; Huang, K. L.; Lagoudas, D. C. Effect of Heat Treatment on Morphology, Crystalline Structure and Photocatalysis Properties of TiO_2 Nanotubes on Ti Substrate and Freestanding Membrane. *Appl. Surf. Sci.* **2011**, *257*, 6451−6461.
(50) Asbrink, G.; Asbrink, S.; Magnéli, A.; Okinaka, H.; Kosuge, K.; Kachi, S. A Ti_3O_5 Modification of V_3O_5-type Structure. *Acta Chem. Scand.* **1971**, *25*, 3889−3890.
(51) Varghese, O. K.; Gong, D. W.; Paulose, M.; Grimes, C. A.; Dickey, E. C. Crystallization and High-Temperature Structural Stability of Titanium Oxide Nanotube Arrays. *J. Mater. Res.* **2003**, *18*, 156−165.
(52) Chae, Y. K.; Mori, S.; Suzuki, M.; Park, J. W. Investigation of Oxygen Adsorption Property of Partially Reduced TiO_2 (TiO_{2-X}). *J. Chem. Eng. Process Technol.* **2011**, *2*, 111−114.
(53) Henderson, M. A.; Epling, W. S.; Perkins, C. L.; Peden, C. H. F. Interaction of Molecular Oxygen with the Vacuum-Annealed TiO_2 (110) Surface: Molecular and Dissociative Channels. *J. Phys. Chem. B* **1999**, *103*, 5328−5337.
(54) Whitemore, D. H.; Kawai, T. Kinetics of Initial Sintering of Vacuum-Reduced Titanium Dioxide. *J. Am. Ceram. Soc.* **1962**, *45*, 375−379.
(55) Epling, W. S.; Peden, C. H. F.; Henderson, M. A.; Diebold, U. Evidence for Oxygen Adatoms on TiO_2 (110) Resulting from O_2 Dissociation at Vacancy Sites. *Surf. Sci.* **1998**, *333*, 412−413.
(56) Shannon, R. D.; Pask, J. A. Kinetics of the Anatase−Rutile Transformation. *J. Am. Ceram. Soc.* **1965**, *48*, 391−398.
(57) Etacheri, V.; Seery, M. K.; Hinder, S. J.; Pillai, S. C. Oxygen Rich Titania: A Dopant Free, High Temperature Stable, and Visible-Light Active Anatase Photocatalyst. *Adv. Funct. Mater.* **2011**, *21*, 3744−3752.